Simulated Diffusion of Phosphorylated CheY through the Cytoplasm of *Escherichia coli*

Karen Lipkow,[1]* Steven S. Andrews,[2] and Dennis Bray[1]

*Department of Anatomy, University of Cambridge, Cambridge, United Kingdom[1],
and Lawrence Berkeley National Laboratory, Berkeley, California[2]*

We describe the use of a computational model to study the effects of cellular architecture and macromolecular crowding on signal transduction in *Escherichia coli* chemotaxis. A newly developed program, *Smoldyn*, allows the movement and interaction of a large number of individual molecules in a structured environment to be simulated (S. S. Andrews and D. Bray, Phys. Biol., in press). With *Smoldyn*, we constructed a three-dimensional model of an *E. coli* cell and examined the diffusion of CheYp from the cluster of receptors to the flagellar motors under control conditions and in response to attractant and repellent stimuli. Our simulations agree well with experimental observations of cell swimming responses and are consistent with the diffusive behavior expected in wild-type and mutant cells. The high resolution available to us in the new program allows us to calculate the loci of individual CheYp molecules in a cell and the distribution of their lifetimes under different cellular conditions. We find that the time delay between stimulus and response differs for flagellar motors located at different positions in the cell. We explore different possible locations for the phosphatase CheZ and show conditions under which a gradient of CheYp exists in the cell. The introduction of inert blocks into the cytoplasm, representing impenetrable structures such as the nucleoid and large protein complexes, produces a fall in the apparent diffusion coefficient of CheYp and enhances the differences between motors. These and other results are left as predictions for future experiments.

Many aspects of the biochemistry and physiology of living cells have in the past been simulated by networks of reactions as though they were electronic circuits. In such studies, components such as receptors, enzymes, or metabolites are portrayed as being wired together in a spatially defined manner through enzymatic and other reactions. But it is clear that living circuitry is not like this; it has unique features such as a highly malleable internal architecture and the existence of a multitude of molecular states that differ in fundamental respects from those of silicon devices. Moreover, the wiring of the cell depends on the diffusive movement of myriad different molecules large and small through the watery interstices of the cytoplasm. In order to understand such systems, we need experimental techniques that can identify individual molecules and track their locations and movements within the cell. Moreover, once data of this kind are obtained we will need advanced computational methods by which spatial locations and diffusive movements of individual molecules can be represented.

We recently developed a computer program for the study of intracellular reactions that allows us to take into account both the spatial location of proteins and protein complexes and their diffusive movements (1). This program uses an approach known as Brownian dynamics, in which molecules are treated as individuals rather than as concentrations and space is treated continuously instead of being subdivided into finite elements (10). Our program is called *Smoldyn*, for Smoluchowski dynamics, because it is based on a theory for the diffusive encounter of molecules in solution developed by the Polish physicist Marjan Smoluchowski (27). Since molecules are treated as individuals, this program can accurately capture stochastic behavior and also simulate diffusive gradients naturally and accurately. We were also inspired in our work by the *MCell* program, which has been developed to account for ionic and molecular events occurring within neuromuscular synapses (32). However, *Smoldyn* has certain advantages over *MCell* for our purposes since it allows reactions to occur between diffusing molecules in solution (in the current version of *MCell*, reactions occur only at membrane surfaces). Moreover, the code of *Smoldyn*, unlike that of *MCell*, is publicly available (http://sahara.lbl.gov/~sandrews/software.html).

In this paper, we describe the application of *Smoldyn* to the well-characterized phenomenon of bacterial chemotaxis in *Escherichia coli*. We first predict the activity of the cluster of chemotactic receptors at one end of the cell in response to different stimulus conditions by using previously described software. We then use the temporal activity profile created in this way as an input to *Smoldyn* to calculate the locations of the diffusing molecules CheY, CheYp, and CheZ within the cell. As a first demonstration of the capabilities of this program, we report a series of simulations in which the diffusion of the signaling protein CheYp is followed through the cell. The behavior we report is in good agreement with analytical solutions but goes far beyond what would be possible to calculate analytically. Moreover, the molecular details revealed by our simulations—such as changing lifetimes of CheYp molecules or the responses of motors at different locations in the cell—exceed the resolution of currently available techniques. We leave them as predictions to be tested in future experiments.

* Corresponding author. Mailing address: Department of Anatomy, University of Cambridge, Downing St., Cambridge CB2 3DY, United Kingdom. Phone: 44-1223-333771. Fax: 44-1223-333786. E-mail: KL280@cam.ac.uk.

MATERIALS AND METHODS

Smoldyn. The *Smoldyn* program is available from http://sahara.lbl.gov/~sandrews/software.html together with a description of the algorithm. A detailed account of the theory and assumptions underlying *Smoldyn* is given in reference 1. Briefly, identified molecules are placed at specific positions within the framework of the simulation volume. The molecules to be simulated are represented in the program as points within the cell box. Some molecules are anchored just inside the walls, whereas others (those that are freely diffusing) are initially assigned random locations. Each molecular species has a diffusion coefficient (which may be zero if it is membrane associated) and a color and size for the graphical animation. The configuration file also includes a list of potential reactions and reaction probabilities. The molecules themselves are point objects and have no dimensions. They are, however, assigned a binding radius for each bimolecular reaction they can undergo, calculated to give the correct reaction rates following a diffusive encounter. At regular intervals, all mobile molecules undergo a diffusive step in a random direction (the step length was 0.1 ms for all of the simulations reported in this paper). Diffusive distances are calculated from Fick's law, converted into probabilities. At the end of this first-simulation step, molecules are moved to their new positions. Any molecule that finds itself inside an excluded volume is returned to its prior position. Molecules that cross the boundary of the cell box are reflected back in, as though they had ballistic trajectories or like light from a mirror. Unimolecular reactions now occur with a probability calculated from the specified rate constant. Bimolecular reactions are decided by the proximity of two potential reactants: two suitable molecules that come within each other's binding radius are made to react. The user can change the system at specific times and record the state of the system as required.

The *E. coli* simulation system. In the studies reported here, we used a rectangular box with a length of 2.5 μm and a width and height of 0.88 μm each (Fig. 1). This has the same volume as an *E. coli* cell with a cylindrical shape and hemispherical ends with a 2.8-μm length and a 1-μm diameter. We have also performed simulations with a more realistic shape, but these are not described here (see cover photo of this issue). The small cells described here were represented by rectangular boxes with dimensions of 1.98 by 0.7 by 0.7 μm, i.e., with the same proportions and 50% of the volume of our standard cell. A square array of 35 by 36 CheA dimers (a total of 1,260) with overall dimensions of 510 by 525 nm is placed 20 nm from the inside surface of the anterior cell wall. Four rings 45 nm in diameter, each made of 34 regularly spaced FliM molecules, are placed on the long sidewalls of the cell; these are positioned 10 nm from the inside surface. We chose to place one ring on a different sidewall every 500 nm along the cell length from the anterior end of the cell, although this is arbitrary since the actual distribution is thought to be random. The 1,600 CheZ dimers of the cell are placed as specified: either all randomly in the cytoplasm and freely diffusing, all in an array 40 nm from the anterior cell wall, or 812 in the anterior array and 788 diffusing freely. The cytoplasm was seeded with 8,200 freely diffusing CheY monomers.

Because of the lack of in vivo data on the activity profile of CheA, we used a separate program (BCT) that uses a set of deterministic rate equations to calculate the concentration of CheA dimers in the receptor cluster and the proportion of active and phosphorylated molecules (4). Details of the BCT program are available at http://www.anat.cam.ac.uk/comp-cell/Chemotaxis.html. Active species were assigned randomly within the designated population to give the required final proportions with the *Smoldyn* equilmol command. Any changes in the input to the cell in the course of a simulation were similarly calculated with BCT. For Fig. 2, the simulation input was the proportion of active CheA dimers (CheA*), which were converted to CheAp in an autophosphorylation reaction in *Smoldyn*. For Fig. 3 to 6, the number of CheAp molecules was read in directly from BCT. The *Smoldyn* program then used the continuous record of phosphorylated CheA dimers to calculate the conversions of individual CheY molecules to CheYp, their diffusion to the motors, and the changes in the occupancy of the FliM rings associated with each of the four motors.

Simulation output. Simulations were run on either an Apple Power Mac G5 (dual 2 GHz, 1.5 gigabytes of random access memory) or an Apple PowerBook G4 (1 GHz, 1 gigabyte of random access memory). For the animations, OpenGL was called from within *Smoldyn* and snapshots were taken with Grab (Apple). For quantifications, the number of molecules of each species at specified time intervals was recorded with the *Smoldyn* command molcount. The exact positions of all CheY and CheYp molecules were recorded with the *Smoldyn* command listmols3. All further analysis of the raw data and plotting was done with MATLAB (The MathWorks, Inc.).

Analytical solutions. Direct calculations of the expected CheYp distribution without simulations were based on the chemical gradient model of Sprague et al. (30), who analyze the spatial distribution of a hypothetical signaling molecule in a spatially segregated kinase-phosphatase system. To include the number of
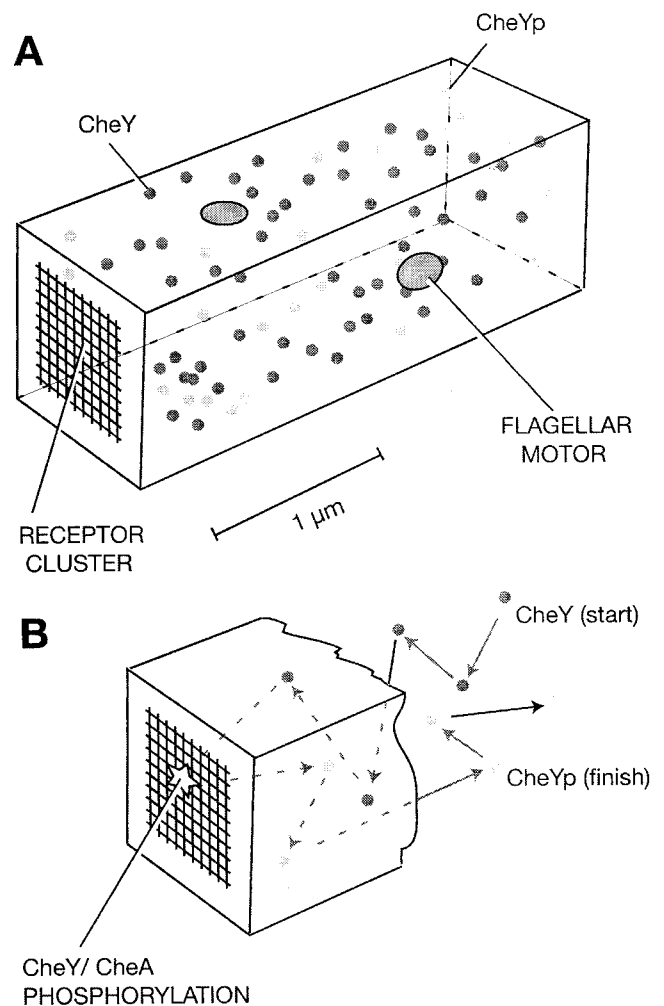

FIG. 1. Basic features of the *E. coli* simulation. (A) In our model, the *E. coli* interior volume is a rectangular box. It contains 8,200 freely diffusing CheY signaling molecules, a small proportion of which is shown here. At any instant, some of these are nonphosphorylated (CheY, black circles) while others are phosphorylated (CheYp, gray circles). The cluster of chemotaxis receptors and associated molecules is represented as an array of 1,260 CheA kinase dimers positioned just inside the receptor cell wall. The flagellar motors are included as four rings of 34 FliM motor switch proteins distributed along the lateral cell walls. CheZ molecules (not shown) can either be associated with the receptor cluster or diffuse freely in the cytoplasm as described in the text. (B) Schematic of phosphorylation events. Any CheY molecule that diffuses within the binding distance of an active phosphorylated CheA molecule itself becomes phosphorylated. The CheYp molecule produced in this way then diffuses back into the cytoplasm (see Fig. 3 for an actual diffusion trace).

phosphorylated kinase molecules explicitly, the first-order heterogeneous (that is, spatially localized) rate constant for the phosphorylation reaction at the cell pole was changed to $k^* = (a_1 N_E)/(1,000 N_A A_C)$, where a_1 is the rate constant for phosphotransfer of CheAp to CheY (10^8 M^{-1} s^{-1}), N_E is the number of CheAp dimers present at any time, N_A is Avogadro's number, and A_C is the cross-sectional area of the cell (in square meters). Note that area rather than volume is used here because the reaction occurs on a two-dimensional surface.

For cells with clustered CheAp and freely diffusing CheZ, k^* was directly substituted into the published equations. In this case, $k = z_1 = 2.2$ s^{-1}, the pseudo-first-order rate constant of CheYp dephosphorylation by CheZ.

For cells with both CheAp and CheZ clustered at the pole, the concentration of CheYp is constant throughout the cell. The fraction of phosphorylated CheY (fp) was calculated from the law of mass action as $fp = [Yp]/([Y] + [Yp]) =$

TABLE 1. Reactions and rate constants

Reaction	Rate constant	Reaction probability/ 0.1-ms time step	Reaction radius (nm) (0.1-ms time steps)	Reference(s)
Unimolecular				
CheA* → CheAp	$3.4 \times 10^1\ s^{-1}$	3.4×10^{-3}		11, 26
CheY → CheYp	$5.0 \times 10^{-5}\ s^{-1}$	0.0^a		15, 22
CheYp → CheY	$8.5 \times 10^{-2}\ s^{-1}$	8.5×10^{-6}		28
FliM · CheYp → FliM + CheYp	$2.0 \times 10^1\ s^{-1}$	2.0×10^{-3}		21, 28
Bimolecular				
CheAp + CheY → CheA* + CheYp	$1.0 \times 10^8\ M^{-1}\ s^{-1}$		16.0	31
CheZ + CheYp → CheZ + CheY	$1.6 \times 10^6\ M^{-1}\ s^{-1}$		4.0	15, 28
FliM + CheYp → FliM · CheYp	$5.0 \times 10^6\ M^{-1}\ s^{-1}$		5.8	21, 28

^{a} At a high temporal resolution, very slow reactions occur in *Smoldyn* with zero probability due to limitations of the random number generator.

$K/(K + 1)$, with $K = k^*/z_1L$, where k^* and z_1 are as above and L is the length of the cell. The introduction of cell length is necessary because both reactions occur on a surface.

Rate constants. Total numbers of molecules per cell are based on recent estimates for strain RP437 in rich medium (15). Binding affinities and rate constants are from the published literature as reported in Table 1 and at http://www.anat.cam.ac.uk/comp-cell/Rates.html. Unless otherwise specified, CheY and CheYp had a diffusion coefficient of 10 $\mu m^2/s$ and CheZ had a diffusion coefficient of 6 $\mu m^2/s$, on the basis of references 9 and 23.

RESULTS

Animations and time courses. Output from a typical *Smoldyn* simulation is shown in Fig. 2. The OpenGL display of an entire cell with its complement of diffusing and nondiffusing molecules is shown for two stimulus conditions: unstimulated (Fig. 2A) and 0.1 s following the addition of a strong repellent (Fig. 2B). A number of changes in response to the repellent stimulus are apparent: the proportion of active and phosphorylated CheA molecules (orange and yellow, respectively) at the anterior cluster rises, and the proportion of phosphorylated CheY molecules (red) rises. There is also an increase in the number of CheYp molecules bound to the FliM rings of the four motors (cyan), although this is difficult to see in these images.

The time course of the cell's response to a pulse of aspartate can be followed in a number of ways, for example, in animations or graphs. Thus, changes in the total CheYp within the cell together with the expected shift in motor occupancy are shown in Fig. 2C. Addition of aspartate causes an initial rapid fall in CheYp, followed by a slow rise to the prestimulus level due to the adaptational mechanism (3, 5). Removal of aspartate at the end of the pulse produces a reciprocal set of changes: a rapid rise in CheYp concentration, followed by a slower fall to the prestimulus condition. These changes in CheYp are mirrored by shifts in the binding of CheYp molecules to the rings of FliM molecules associated with the inner face of each flagellar motor and hence the rotational bias—the fraction of time a motor spends in counterclockwise rotation.

Diffusion traces. An important feature of the *Smoldyn* program is its ability to trace the movements of individual protein molecules diffusing through the cytoplasm. The specimen result shown in Fig. 3A displays the diffusive motion of a single CheY molecule within the cell. The entire path shown here occupied 100 ms, revealing the ability of protein molecules to visit most regions of the cell within a remarkably short period

of time. The second molecule shown in Fig. 3B happened to encounter the cluster of CheA molecules at the anterior end of the cell, where it was converted to the phosphorylated form (CheYp, gray).

CheZ localization. The output from the *Smoldyn* simulation can also be used to collect statistical information on different molecules. For example, in Fig. 4 we show the lifetimes of CheYp molecules—that is, the duration in seconds between their formation at the anterior cluster of CheA molecules and their loss by encounter with a CheZ molecule. The analysis was performed for three cytological distributions of CheZ: all localized close to the inner face of the CheA cluster (Fig. 4A), uniformly dispersed in a freely diffusing form throughout the cytoplasm (Fig. 4B), and equally divided between the cluster and the cytoplasm (Fig. 4C). In all cases, the mean lifetime of CheYp molecules is very close to the expected lifetime of $1/(2.2\ s^{-1}) = 0.455$ s, calculated from the CheZ-mediated dephosphorylation rate in vivo, which confirms the validity of the system. In addition to the determination of mean lifetimes, which is equivalent to the bulk measurements done experimentally, our simulations allow an analysis of the detailed distribution of the lifetimes of single molecules.

As may be seen, the polar location of CheZ produces a larger proportion of CheYp molecules with a very short (that is, less than 0.1 s) lifetime. Evidently, a significant population of CheY molecules, associated with the receptor cluster, cycles rapidly in a futile cycle between a phosphorylated state and a dephosphorylated state. On the other hand, the number of molecules with a very long lifetime (longer than 2 s) is also increased in cells with polar CheZ. This makes sense, as molecules that have escaped the influence of the CheA/CheZ cluster on the anterior cell pole will not encounter another phosphatase molecule until they diffuse back toward the anterior pole. In cells with CheZ shared between the cluster and the cytoplasm (Fig. 4C), the number of very short lifetimes lies between the two extremes, as expected. Interestingly, the mean lifetime of CheYp molecules is shortest in this last case (Fig. 4 insets).

We examined the distribution of CheYp molecules within the cytoplasm and the changes produced by the localization of CheZ. When CheZ molecules were restricted to the receptor cluster at the anterior pole of the cell, the distribution of CheYp was essentially uniform in the cytoplasm (Fig. 5A). However, when the same number of CheZ molecules was
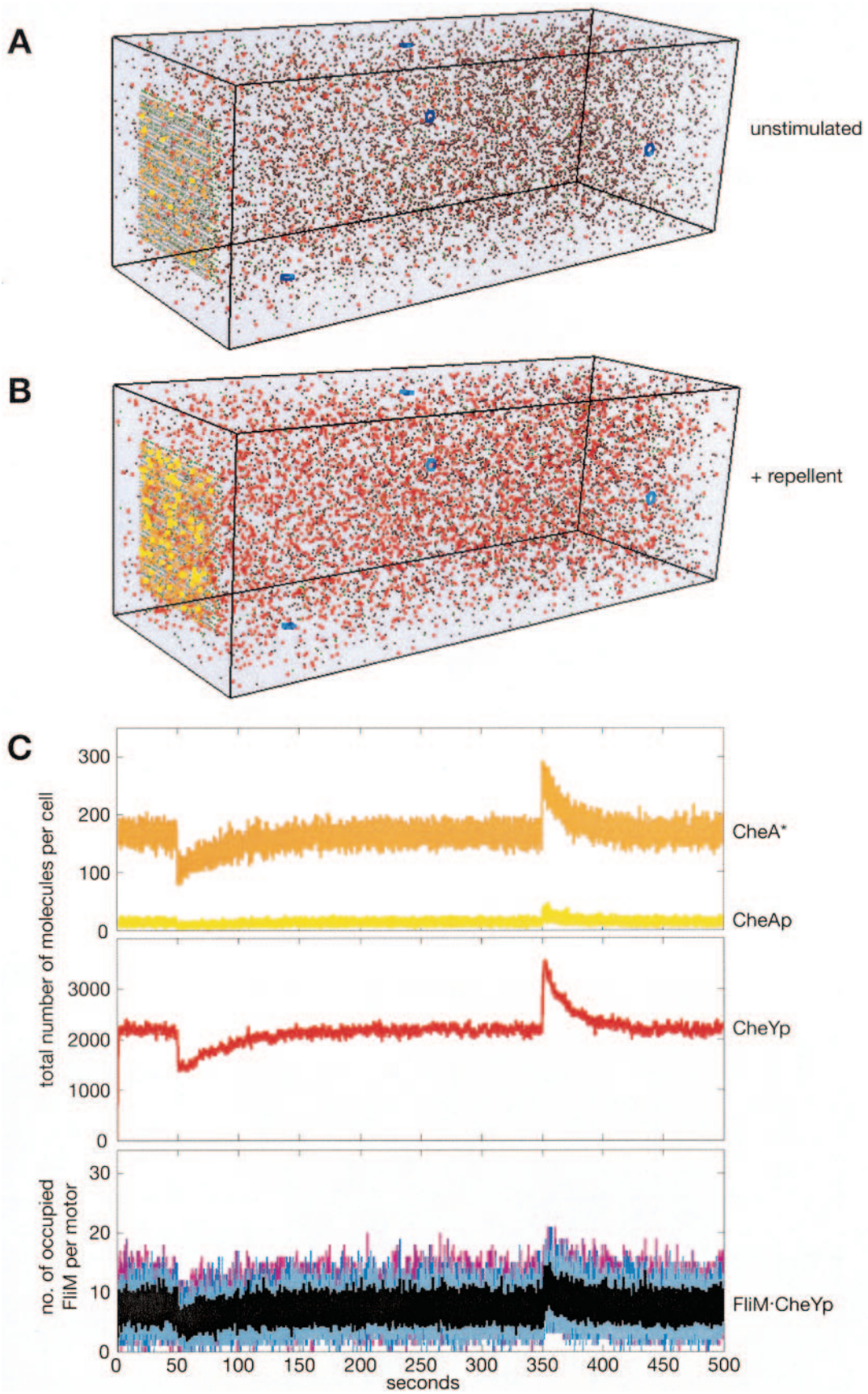
allowed to diffuse freely, then the distribution of CheYp showed an exponential gradient highest at the anterior end, where CheYp molecules are produced (Fig. 5B). The same effect was even more dramatic when we arbitrarily reduced the diffusion coefficients of CheY, CheYp, and CheZ molecules by a factor of 10 (Fig. 5C). For the wild-type diffusion coefficients, there was excellent agreement between the simulations and analytical solutions of the problem (dashed lines).

Cell dimensions. The *Smoldyn* chemotaxis model can be used to explore the consequences of different cellular architectures on the diffusion of CheYp and hence the chemotaxis performance. For example, we found pronounced effects due to the dimensions of the cell. Assuming that the cell had the same number of molecules and all reactions proceed at the same rate, reducing the cytoplasmic volume increases the density of all of the molecules and shortens the distances of diffusion. Thus, we found that a reduction in cell volume of 50% caused a decrease in CheY lifetime to 58% and a decrease in CheYp lifetime to 47% (Fig. 4D). Consequently, we found a reduction in resting CheYp (averaged over the cell) of 9%, and the steady-state level was reached more quickly (not shown). If the number of molecules varies in proportion to the cell volume (that is, concentrations remain unchanged), CheY and CheYp lifetimes show only modest changes in distribution (not shown).

Motor positioning. We also found small effects due to the positioning of the flagellar motors in the cell. In our model, four flagellar motors are positioned at 0.5, 1.0, 1.5, and 2.0 μM from the anterior end. If the CheA molecules at this end are instantaneously activated (equivalent to their occupation by a repellent), then a wave of CheYp travels into the cell. The high temporal resolution available in the *Smoldyn* program reveals a small time delay in the arrival of this wave at the flagellar motors, recorded as a rise in the binding of CheYp to the FliM molecules of the motor C ring. There is a small but significant difference in the time of arrival at the different motors (Fig. 6E).

Macromolecular crowding. In the *Smoldyn* simulation, individual molecules are represented as dimensionless points; they have position but not size. However, we know that the actual cytoplasm is a highly crowded environment (16, 17). A diffusing molecule can be hindered by large aggregates of proteins and other macromolecules for steric reasons, as well as by possible binding interactions. In order to attempt to represent these constraints in our program, we have introduced an array of impenetrable blocks into the cytoplasm of our simulated cell (Fig. 6B). The effect of these obstacles is to reduce the efficiency of diffusive movement. This results in an increased steepness of the CheYp gradient in simulations with cytoplasmic CheZ (Fig. 6C and D) and a further spreading of the response time of the four motors (Fig. 6E
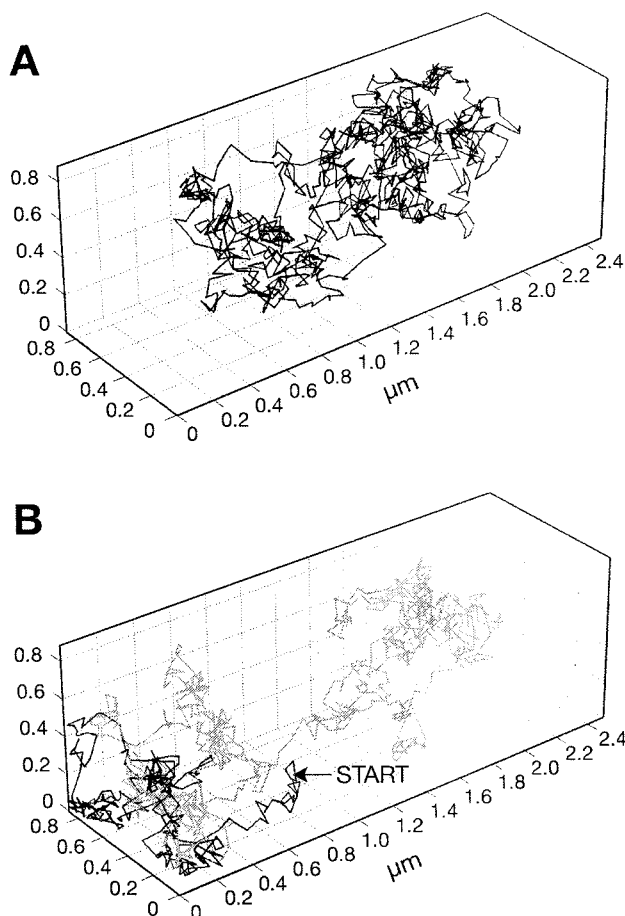

FIG. 3. Loci of CheYp molecules. (A) Three-dimensional trace of an individual CheY molecule followed at a 0.1-ms resolution for 100 ms. Note that this time is sufficient for the protein molecule to travel from one end of the cell to the other. (B) Another 100-ms trace. In this case, the CheY molecule (black) happened to encounter the cluster of CheA molecules at the anterior end of the cell, where it became phosphorylated (gray).

and F). Presumably, at the anterior end, where CheY is phosphorylated, crowding increases the local concentration of CheYp and therefore accelerates the response of the anterior-most motor. At the other, posterior, end of the cell, the local CheYp concentration is reduced by the need to diffuse through the obstacles and the responses of motors in this region is consequently delayed.

DISCUSSION

We have shown in this report that it is feasible to simulate the entire population of diffusing molecules in the chemotactic

---

FIG. 2. Sample output from the *Smoldyn* program. One optional output from the Smoldyn program is an OpenGL movie from which individual images (snapshots) can be taken. (A) Snapshot image of a cell in steady state in the absence of stimulation. Color codes: gray, CheA (inactive conformation); orange, CheA* (active conformation); yellow, CheAp (active conformation, phosphorylated); green, CheZ; dark brown, CheY; red, CheYp; blue, FliM; cyan, FliM · CheYp. (B) Same cell 0.1 s after addition of a saturating repellent stimulus. The color codes are the same as in panel A. (C) Time course showing changes in the level of CheYp in response to a 300-s pulse of 10 μM aspartate. The proportion of active CheA* molecules was updated every 100 ms, and the number of molecules of each species was determined every 10 ms. At the bottom, the four motors are shown in different colors and the mean of the four motors is in black.
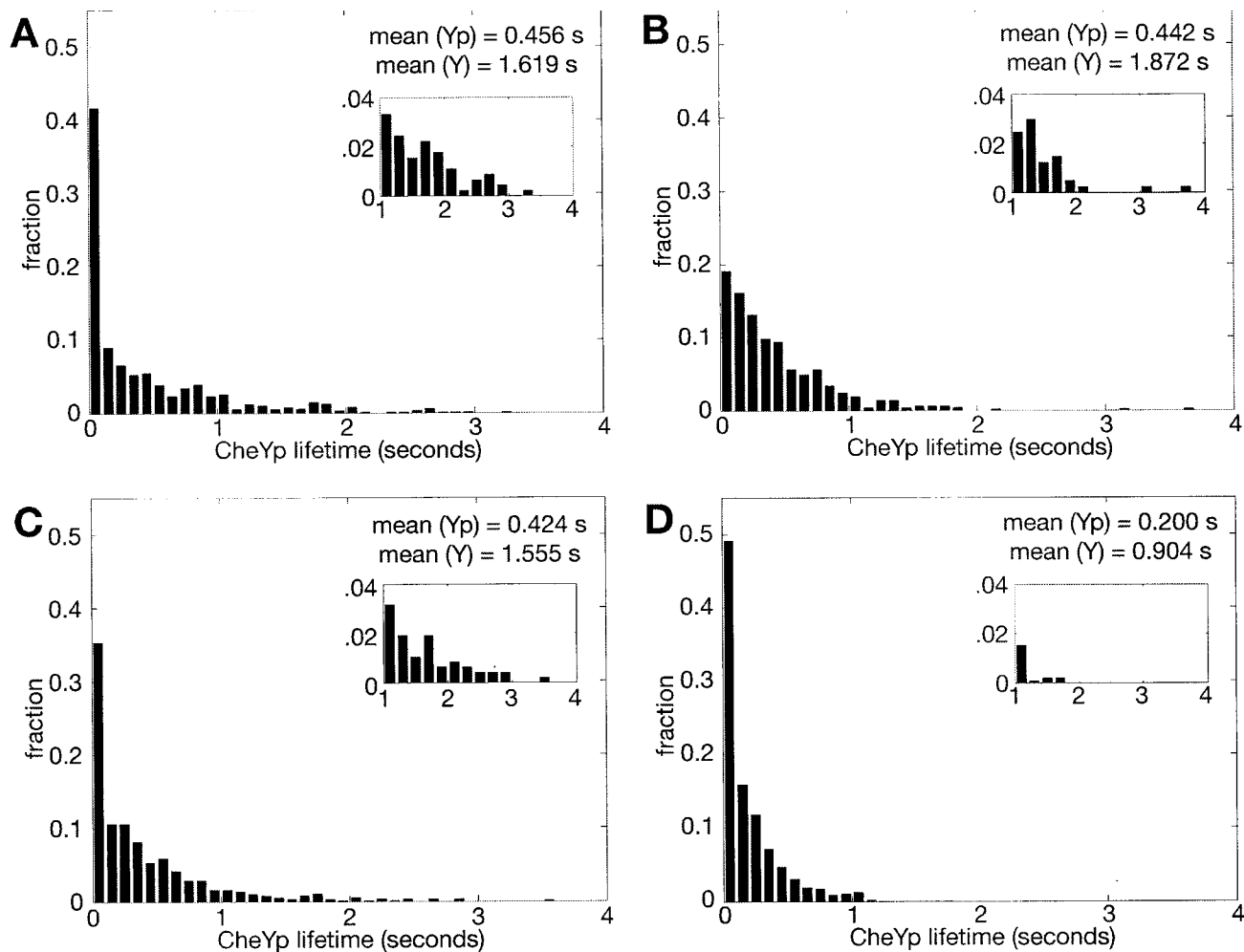
FIG. 4. Lifetimes of CheYp molecules. Histograms show the lifetimes of phosphorylated CheYp in a cell with CheZ with three different distributions within the cell: A, polar (localized to the cluster of receptors at the anterior end of the cell); B, free (diffusing freely within the cytoplasm); C, mixed (50% of CheZ molecules associated with the receptor cluster and 50% diffusing freely). D is a small cell with 50% of the cell volume but the same molecule numbers as in panels A to C and a mixed CheZ distribution. Simulations were run for 1,000 s (10^7 time steps) with a single molecule of CheY, recording the identity of this molecule at every time step. Molecules that became phosphorylated in the simulation were followed until they were eventually dephosphorylated, thereby giving a histogram of lifetimes of CheYp. Note that these include the time spent bound to the flagellar motors. The main diagrams show the entire spread of CheYp lifetimes obtained, in 0.1-s bins. The insets show CheYp lifetimes of more than 1 s on a different scale. The average lifetimes of CheY and CheYp under different conditions are given in seconds.

pathway of *E. coli*. The estimated 6,000 CheY molecules, 2,200 CheYp molecules and, where appropriate, 1,600 CheZ molecules can all be monitored as they diffuse and react within the confines of the bacterial plasma membrane. Their changes in response to external stimuli acting on the cluster of receptors at the anterior end of the cell and the consequent changes in the flagellar motors are all consistent with experimental records. Thus, we found that the delay time between a sudden stimulus at the anterior cluster of CheA molecules and a rise in the occupancy of CheYp molecules at the flagellar motors to half saturation is around 100 to 300 ms. This is in broad agreement with experimental measurements of this delay time (13, 24, 28). With the higher resolution available to us, we could also detect small differences in the response times of different motors depending on their positions in the cell. The time delays are on the order of 50 ms, which seems unlikely to have an appreciable affect on the overall performance of the

cell. However, we can see that if CheYp had a lower diffusion constant then signaling times would produce a significant delay.

Protein localization and crowding. There is uncertainty regarding the precise location of CheZ in the *E. coli* cell. On the one hand, fluorescent images obtained with protein labeled with green fluorescent protein reveal that a significant fraction of CheZ is localized at the cluster of receptors at one end of a cell (7, 29). On the other hand, biochemical experiments are consistent with a protein that is dimeric in solution and undergoes oligomerization in the presence of CheYp (2). In the light of this uncertainty, we tested the effects of three possible distributions of CheZ: (i) all polar, (ii) all cytoplasmic, and (iii) partly polar and partly cytoplasmic. One result was that cells with polar CheZ have a larger fraction of CheYp molecules with a very short lifetime (less than 0.1 s). We interpret this transient population as evidence of rapid futile recycling be-
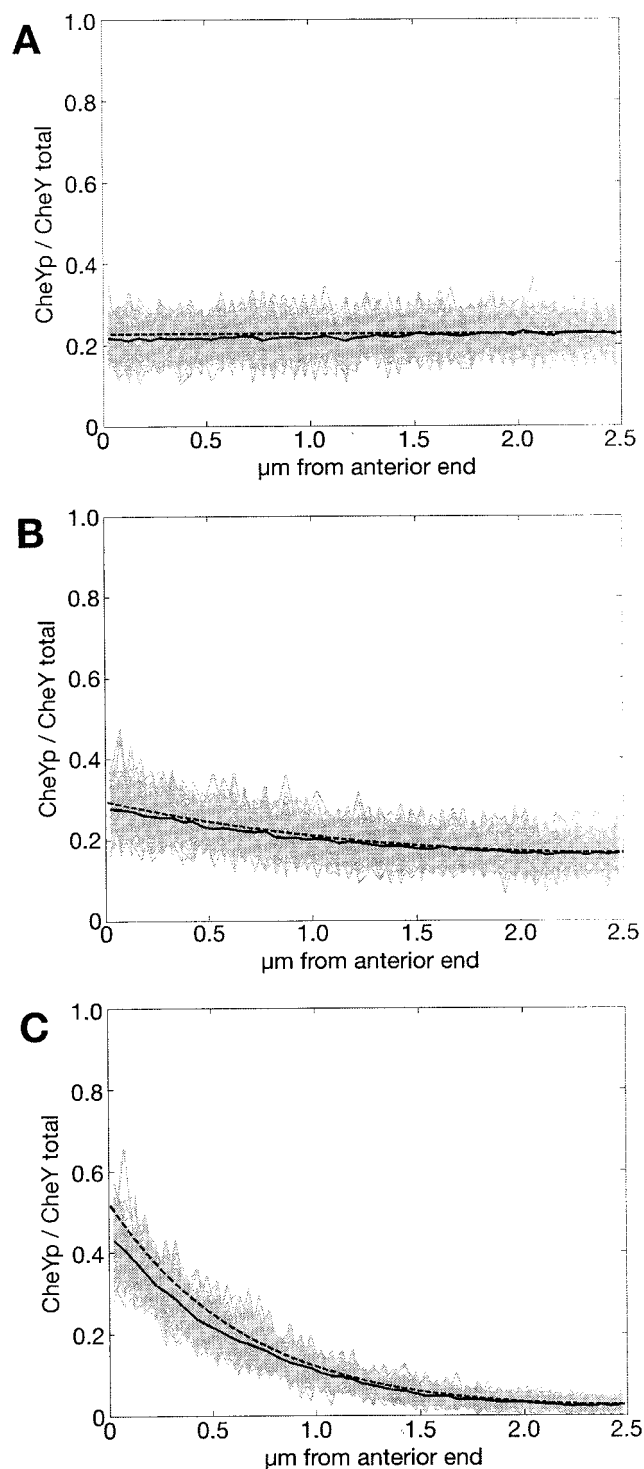
FIG. 5. Gradients of CheYp. The distribution of CheYp molecules in an unstimulated cell was examined in serial slices through the cell taken at intervals of 50 nm along its long axis. Numbers of CheYp molecules are shown here for 100 snapshots of the cell (gray lines) and the mean of these instantaneous records (black lines). Black dashed lines show the analytical solution based on the diffusion equation, modified from reference 30. (A) Diffusion coefficients for CheY and CheYp, both 10 $\mu m^2/s$. CheZ is localized at the polar cluster. (B) Diffusion coefficients for CheY and CheYp, both 10 $\mu m^2/s$. CheZ is freely diffusing in the cytoplasm at 6 $\mu m^2/s$. (C) Diffusion coefficients for CheY and CheYp both reduced to 1 $\mu m^2/s$. CheZ is diffusing at 0.6 $\mu m^2/s$.

tween CheY and CheYp in the vicinity of the receptor cluster. A second result was the formation of a gradient of CheYp in the cytoplasm when CheZ was allowed to diffuse freely through the cell. In this case we saw a pronounced exponential decrease in CheYp from the site of formation at the anterior end of the cell (Fig. 5). A gradient of this kind has been predicted to occur when a kinase (in this case, CheA) is immobilized in one region of the cell and a cognate phosphatase (equivalent to CheZ) is freely diffusing in the cytoplasm (6). Quantitative predictions of the shape of this gradient with analytical methods based on classical diffusion theory gave good agreement with our stochastic simulations with *Smoldyn* (8, 30). Recent experimental evidence has been obtained to show the existence of gradients of phosphorylated protein (in this case, the microtubule-binding protein stathmin) in the cytoplasm of cells undergoing mitosis (19). Although the gradients of CheYp predicted in our simulations are quite shallow because of the small size of the bacterial cell, they could become significant if the diffusion coefficient of CheY became significantly reduced.

It therefore seems that the chemotaxis performance of *E. coli* is pushed close to the limit imposed by the diffusion coefficients of its signaling molecules, especially CheYp. This conclusion is underscored by our attempts to replicate the crowded conditions of the cell interior. The presence of very high concentrations of proteins and other macromolecules (in excess of 300 mg/ml) (20) and their pronounced tendency to associate into large oligomeric or polymeric structures must place innumerable obstacles in the path of any diffusing molecule. Although we do not know the actual topology of the cytoplasm we tried, as a first step, to see what would happen if we distributed numerous small boxlike obstacles throughout the cell. A total of 12,544 cubic obstacles in a regular square lattice, taking up 41% of the cell volume, produced an approximately twofold decrease in the diffusion coefficient of CheYp. As already noted, this reduction would be sufficient to cause significant delays in the activation of distant flagellar motors.

Outlook. In the present study we used a relatively simple deterministic program to calculate the input to the *Smoldyn* program. The BCT program performs numerical integration of the rate constants of some 60 biochemical reactions: We used it to calculate the number of active CheA molecules at any instant of time, which was then fed into the *Smoldyn* simulation. With the current implementation, the complement of active CheA molecules was distributed to random positions within the square array. However, it would be possible to encode more information regarding the positions of these active CheA molecules. For example, the StochSim program developed previously provides a much more detailed picture of dynamic changes occurring in the cluster of receptors on the surface of an individual cell (18). It successfully accounts for both the amplification produced by the cluster of the receptors and the temporal distribution of run lengths seen in individual flagellar motors (14). Moreover, use of this program has led to the prediction of spatial patterns of activation due to receptor coupling within the cluster (25). It would be a straightforward matter to take the dynamic output from a StochSim program and use it as the input for a *Smoldyn* simulation. We would then be able to examine the effects not only of the numbers of active CheA molecules but also of their spatial distribution.
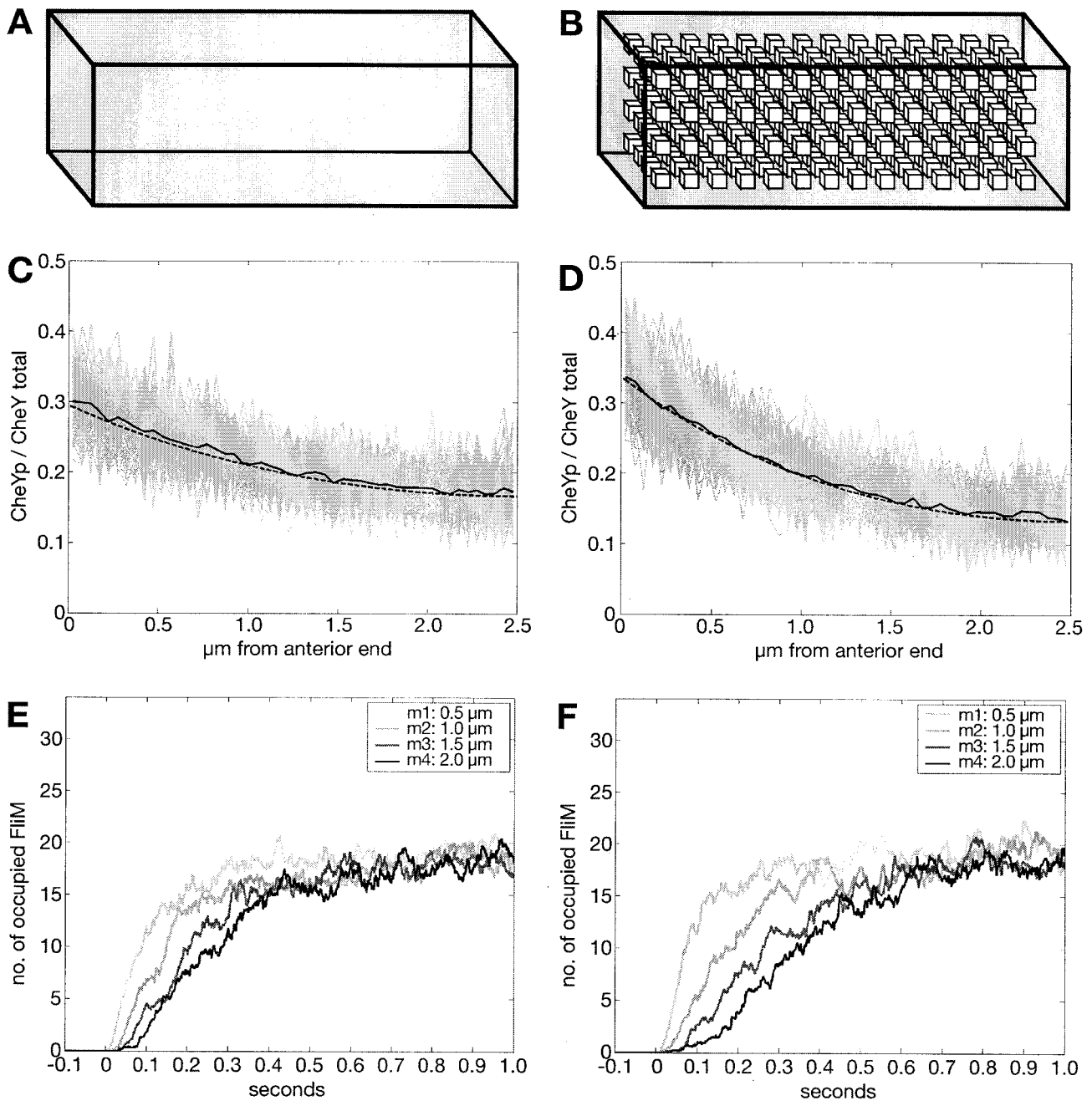
FIG. 6. Cytoplasmic obstructions. (A) Schematic of an uncrowded cell, in contrast to that in panel B, a crowded cell in which a large number of obstacles (small cubes) is placed into the cytoplasm. These are meant to represent the diffusive barriers caused by structures such as the nucleoid or large multiprotein complexes. The drawing is for illustration only; in the simulation, 12,544 cubic exclusion boxes with an edge length of 40 nm were placed into a regular array with 10-nm gaps between the boxes and 30-nm gaps between boxes and cell walls. The edge length of each box is approximately equivalent to the diameter of a ribosome plus the diameter of a CheY molecule (to make up for molecules not having a volume in the simulations) (12, 33). The total volume taken up by the exclusion boxes is equivalent to the level of macromolecular crowding in a typical bacterial cell. (C) Distribution of CheYp without cytoplasmic obstructions. Both CheY and CheZ were freely diffusing in the cytoplasm and had diffusion coefficients of 10 and 6 $\mu m^2/s$, respectively. The analytical solution (dashed line) was also generated with a diffusion coefficient of 10 $\mu m^2/s$. Histograms of CheYp distribution were generated as for Fig. 5, but note the difference in scale. (D) Same CheYp distribution as in panel C but with cytoplasmic obstructions that are shown to cause a significant delay in diffusion and the establishment of a steeper concentration gradient. The simulation was done with the same diffusion coefficients as in panel C, but the analytical solution used a diffusion coefficient of 5.5 $\mu m^2/s$ to fit the simulation. (E and F) Change in motor occupancy in response to a sudden rise in CheA activity in the absence (E) and presence (F) of crowding. m1, motor 1, placed 0.5 μm from anterior pole, etc. At $t = 0$, the proportion of phosphorylated CheA was raised from 0 to 100%, resulting in a constant supply of CheYp being generated at the anterior pole and diffusing through the cell. The traces shown are means of 10 simulation runs.

Our experience with *Smoldyn* encourages us to think that programs of this kind will be used to answer a range of questions relating to diffusive events in bacterial chemotaxis. Thus, we have already examined the distribution of CheYp molecules in the cell and found conditions under which there should be a gradient of CheYp molecules, decreasing from the receptor plaque. Further investigations along these lines should permit us to learn more about these gradients. How will the gradient change with external stimulation? Could there be conditions (for example, following a sudden increase or decrease in some attractant) under which waves of CheYp sweep across a cell? If so, how large will the waves be and how fast will they travel? Might there also be concentration gradients of other protein components of the pathway, such as CheZ? If so, how will these affect chemotactic performance?

Since the *Smoldyn* program monitors individual molecules with a high level of time resolution, it is an ideal vehicle to address issues of stochasticity and noise in the chemotactic pathway. How will noise at the front end of the system (that is, in the input stimulus) propagate through the system? If the cluster of receptors were to generate temporal pulses or regional patterns of activation (as suggested above), what effect, if any, would this have on downstream signals? At the other end of the pathway, we can ask whether the binding of CheYp molecules to the motor will significantly change the local concentration of CheYp. Could this act as a feedback mechanism to regulate signal strength in accordance with motor rotation? How large will the fluctuations in CheYp be in the vicinity of the motor? How will these fluctuations influence the stochastic transitions of the motor from clockwise to counterclockwise rotation? What is the working range of CheYp concentrations in the vicinity of a motor (going from completely clockwise to completely counterclockwise), and how precisely does this have to be specified by the cell? Is the adaptation system competent to maintain CheYp concentrations within this range, or could there be other mechanisms at play?

REFERENCES

1. **Andrews, S. S., and D. Bray.** 2004. Stochastic simulation of chemical reactions with spatial resolution and single molecule detail. Phys. Biol. **1:**137–151.
2. **Blat, Y., and M. Eisenbach.** 1994. Phosphorylation-dependent binding of the chemotaxis signal molecule CheY to its phosphatase, CheZ. Biochemistry **33:**902–906.
3. **Bourret, R. B., and A. M. Stock.** 2002. Molecular information processing: lessons from bacterial chemotaxis. J. Biol. Chem. **277:**9625–9628.
4. **Bray, D., and R. B. Bourret.** 1995. Computer analysis of the binding reactions leading to a transmembrane receptor-linked multiprotein complex involved in bacterial chemotaxis. Mol. Biol. Cell **6:**1367–1380.
5. **Bren, A., and M. Eisenbach.** 2000. How signals are heard during bacterial chemotaxis: protein-protein interactions in sensory signal propagation. J. Bacteriol. **182:**6865–6873.
6. **Brown, G. C., and B. N. Kholodenko.** 1999. Spatial gradients of cellular phospho-proteins. FEBS Lett. **457:**452–454.
7. **Cantwell, B. J., R. R. Draheim, R. B. Weart, C. Nguyen, R. C. Stewart, and M. D. Manson.** 2003. CheZ phosphatase localizes to chemoreceptor patches via CheA-short. J. Bacteriol. **185:**2354–2361.
8. **Crank, J.** 1975. The mathematics of diffusion, 2nd ed. Oxford University Press, Oxford, United Kingdom.
9. **Elowitz, M. B., M. G. Surrette, P.-E. Wolf, J. B. Stock, and S. Leibler.** 1999. Protein mobility in the cytoplasm of *Escherichia coli.* J. Bacteriol. **181:**197–203.
10. **Ermak, D. L., and J. A. McCammon.** 1978. Brownian dynamics with hydrodynamic interactions. J. Chem. Phys. **69:**1352–1360.
11. **Francis, N. R., M. N. Levit, T. R. Shaikh, L. A. Melanson, J. B. Stock, and D. J. DeRosier.** 2002. Subunit organization in a soluble complex of tar, CheW, and CheA by electron microscopy. J. Biol. Chem. **277:**36755–36759.
12. **Gabashvili, I. S., R. K. Agrawal, C. M. Spahn, R. A. Grassucci, D. I. Svergun, J. Frank, and P. Penczek.** 2000. Solution structure of the *E. coli* 70S ribosome at 11.5 Å resolution. Cell **100:**537–549.
13. **Khan, S., J. L. Spudich, J. A. McCray, and D. R. Trentham.** 1995. Chemotactic signal integration in bacteria. Proc. Natl. Acad. Sci. USA **92:**9757–9761.
14. **Korobkova, E., T. Emonet, J. M. Vilar, T. S. Shimizu, and P. Cluzel.** 2004. From molecular noise to behavioural variability in a single bacterium. Nature **428:**574–578.
15. **Li, M., and G. L. Hazelbauer.** 2004. Cellular stoichiometry of the components of the chemotaxis signaling complex. J. Bacteriol. **186:**3687–3694.
16. **Luby-Phelps, K.** 2000. Cytoarchitecture and physical properties of cytoplasm: volume, viscosity, diffusion, intracellular surface area. Int. Rev. Cytol. **192:**189–221.
17. **Minton, A. P.** 2001. The influence of macromolecular crowding and macromolecular confinement on biochemical reactions in physiological media. J. Biol. Chem. **276:**10577–10580.
18. **Morton-Firth, C. J., T. S. Shimizu, and D. Bray.** 1999. A free-energy-based stochastic simulation of the Tar receptor complex. J. Mol. Biol. **286:**1059–1074.
19. **Niethammer, P., P. Bastiaens, and E. Karsenti.** 2004. Stathmin-tubulin interaction gradients in motile and mitotic cells. Science **303:**1862–1866.
20. **Record, M. T., Jr., E. S. Courtenay, D. S. Cayley, and H. J. Guttman.** 1998. Responses of *E. coli* to osmotic stress: large changes in amounts of cytoplasmic solutes and water. Trends Biochem. Sci. **23:**143–148.
21. **Sagi, Y., S. Khan, and M. Eisenbach.** 2003. Binding of the chemotaxis response regulator CheY to the isolated, intact switch complex of the bacterial flagellar motor: lack of cooperativity. J. Biol. Chem. **278:**25867–25871.
22. **Schuster, M., R. E. Silversmith, and R. B. Bourret.** 2001. Conformational coupling in the chemotaxis response regulator CheY. Proc. Natl. Acad. Sci. USA **98:**6003–6008.
23. **Segall, J. E., A. Ishihara, and H. C. Berg.** 1985. Chemotactic signaling in filamentous cells of *Escherichia coli.* J. Bacteriol. **161:**51–59.
24. **Segall, J. E., M. D. Manson, and H. C. Berg.** 1982. Signal processing times in bacterial chemotaxis. Nature **296:**855–857.
25. **Shimizu, T. S., S. V. Aksenov, and D. Bray.** 2003. A spatially extended stochastic model of the bacterial chemotaxis signalling pathway. J. Mol. Biol. **329:**291–309.
26. **Shrout, A. L., D. J. Montefusco, and R. M. Weis.** 2003. Template-directed assembly of receptor signaling complexes. Biochemistry **42:**13379–13385.
27. **Smoluchowsky, M. V.** 1916. Versuch einer mathematischen Theorie der Koagulationskinetik kolloider Lösungen. Z. Phys. Chem. **92:**129–168.
28. **Sourjik, V., and H. C. Berg.** 2002. Binding of the *Escherichia coli* response regulator CheY to its target measured *in vivo* by fluorescence resonance energy transfer. Proc. Natl. Acad. Sci. USA **99:**12669–12674.
29. **Sourjik, V., and H. C. Berg.** 2000. Localisation of components of the chemotaxis machinery of *Escherichia coli* using fluorescent protein fusions. Mol. Microbiol. **37:**740–751.
30. **Sprague, B. L., C. G. Pearson, P. S. Maddox, K. S. Bloom, E. D. Salmon, and D. J. Odde.** 2003. Mechanisms of microtubule-based kinetochore positioning in the yeast metaphase spindle. Biophys. J. **84:**3529–3546.
31. **Stewart, R. C., K. Jahreis, and J. S. Parkinson.** 2000. Rapid phosphotransfer to CheY from a CheA protein lacking the CheY-binding domain. Biochemistry **39:**13157–13165.
32. **Stiles, J. R., and T. M. Bartol.** 2001. Monte Carlo methods for simulating realistic synaptic microphysiology using MCell, p. 87–127. *In* E. De Schutter (ed.), Computational neuroscience: realistic modeling for experimentalists. CRC Press, Inc., Boca Raton, Fla.
33. **Volz, K., and P. Matsumura.** 1991. Crystal structure of *Escherichia coli* CheY refined at 1.7-Å resolution. J. Biol. Chem. **266:**15511–15519.